DYNAMIC LATERAL STABILITY OF ELASTOMERIC SEISMIC ISOLATION BEARINGS

V. S. M. Vemuru[1], S. Nagarajaiah[2*], A. Masroor[3], G. Mosqueda[4]

Abstract *Predicting the response of elastomeric seismic isolation bearings when subjected to severe ground motions is challenging due to the highly nonlinear behavior associated with the bearings under a combination of large displacements and axial loads. In particular, the horizontal stiffness of the bearings is a function of both horizontal displacement as well as axial load that varies due to overturning moments. Previous analytical models or formulations to model these bearings were mainly developed to estimate critical loads at the stability limit. Only few of these models are capable of estimating the correct nonlinear behavior of bearings observed at horizontal displacements in excess of the bearing width. In this study, a nonlinear analytical model is presented that is capable of modeling the dynamic response of bearings more accurately at all displacement ranges, especially beyond the stability limit and is verified with experimental data from an earlier experimental study. It was observed in the dynamic experiments that the bearings have a far larger capability to sustain horizontal loads at displacements exceeding their stability limit than predicted by earlier models and more importantly the bearings re-centered after these large displacement excursions. This behavior is captured using the analytical model developed in this study.*

INTRODUCTION

Base isolation has become a widely accepted technique in structural engineering over the past three decades for protecting structures from severe ground motion. Lead rubber bearings and spherical sliding

[1] PhD Candidate, Rice University, Houston, TX – 77005, USA, svv1@rice.edu
[2] Professor, Rice University, Houston, TX – 77005, USA, satish.nagarajaiah@rice.edu
[*] corresponding author
[3] PhD Candidate, University at Buffalo (SUNY), Buffalo, NY – 14260, USA, am249@buffalo.edu
[4] Associate Professor, University of California, San Diego, CA – 92093, USA, gmosqueda@ucsd.edu

bearings constitute the most widely used seismic protection technology. Due to their inherent flexibility in the horizontal direction, the bearings have the capacity to undergo large displacements when subjected to strong ground motion. Under a combination of large displacements and varying axial loads, the behavior of elastomeric bearing becomes highly nonlinear. Under such circumstances the horizontal stiffness of the bearings becomes a nonlinear function of axial load and lateral displacement.

The theoretical approaches adopted by researchers to address stability of elastomeric bearings (Derham & Thomas, 1981; Gent, 1964) made use of Haringx's theory (Haringx, 1948; Haringx, 1949a; Haringx, 1949b) of flexible columns. Both the studies predicted decrease in horizontal stiffness of the bearings with increasing axial load. Buckle and Kelly (1986) conducted experimental studies on a scaled bridge model equipped with slender elastomeric bearings. Koh and Kelly (1988) developed a two-spring mechanical model that takes into account the influence of axial load on horizontal stiffness of bearings, and also a viscoelastic stability model (Koh and Kelly, 1989) for elastomeric bearings. The use of Haringx's type formulation for modeling the stiffness of elastomeric bearings is found to be closer to experimental results (Bažant, 2003; Bažant & Cedolin, 1991).

Nagarajaiah and Ferrell (1999) proposed an enhanced nonlinear model based on the linear two-spring model developed by Koh and Kelly (1988). In their study the authors demonstrate the ability of the analytical model to capture the force-displacement behavior of elastomeric bearings when subjected to large axial loads and horizontal displacements. Further they also show that the critical load of the bearings reduced with increasing horizontal displacement and the horizontal stiffness decreases with increasing horizontal displacement and axial load. Nagarajaiah and Ferrell (1999) validated and verified their analytical model using results from the experimental study performed by Buckle and co-wokers. These experimental results were later documented in the paper by Buckle et al. (2002). Iizuka (2000) proposed a macroscopic model for predicting the response of laminated rubber bearings at large deformations. The model proposed by Iizuka (2000) was also a modified version of the two-spring model proposed by Koh and Kelly (1989), where the linear springs were replaced with non-linear springs. The author Iizuka

(2000) determines the nonlinear parameters of the rotational and shear spring empirically from results of basic load testing on laminated rubber bearings. Kikuchi et al. (2010) developed a new analytical model comprising of multiple shear springs at the mid-height and a series of axial springs at the top and bottom boundaries of the model. Their work predominantly focuses on square seismic isolation bearings and they highlight the importance loading direction has on the ultimate behavior of the bearings. Weisman and Warn (2012) present experimental testing and detailed nonlinear finite element analysis for investigating the critical load capacities of elastomeric and lead-rubber bearings at large lateral displacements. They performed a parametric study to investigate the dependency of critical load on bearing geometry (Warn and Weisman 2011). Cardone and Perrone (2012) also reported critical loads from experiments performed on slender elastomeric bearings.

A recent study by Sanchez et al. (2012) focuses on an experimental testing program to examine the behavior of elastomeric bearings at and beyond their stability limit. Based on quasi-static tests performed on three different types of reduced scale elastomeric bearings, the authors conclude that the reduced area formula (Sanchez et al. 2012) based on effective shear modulus at 25% shear strain is more accurate in predicting the critical loads of bearings. The authors also note the ability of the bearings to recover from motions exceeding their stability limits during dynamic tests and identify the critical load and shear strain limits below which instability in the bearings is unlikely to occur. Han et al. (2013) studied in a detailed manner the controlling mechanism that governs the critical loads in elastomeric bearings. They compare the capability of two different analytical models: Nagarajaiah and Ferrell (1999) and Iizuka (2000) models, for predicting the critical loads and displacements of elastomeric isolation bearings. They perform a global sensitivity analysis on the model parameters and identify that the prediction is most sensitive to the nonlinear behavior of the rotational spring for lateral displacements greater than 0.6 times bearing diameter/width. Han et al. (2013) propose a modified analytical model based on the sensitivity analysis using fewer empirical parameters that has similar predictive capabilities as that of Iizuka (2000) model.

While recent analytical studies have provided considerable insight into the nonlinear behavior of bearings, instances of rollover or instability were observed during pervious experimental studies. Buckle and Kelly (1986) experimentally studied the dynamic performance of slender elastomeric bearings in an isolated bridge deck model. The bearings were dowelled and experienced partial and complete rollover during dynamic testing. Griffith et al. (1987) conducted experiments on a quarter scale nine-story isolated test model to study the effectiveness of an uplift restraint device. In certain test cases where restraints were not installed, column uplift was observed and the force-displacement loops of supporting bearing appear to become unstable due to a sudden drop in stiffness.

Particularly for performance-based design, it is important to extend the theoretical understanding on the stability of elastomeric bearings based on static/quasi-static tests to dynamic behavior and enhance our ability to predict their response when subjected to extreme earthquake loading. In this study an enhanced analytical model is developed based on the nonlinear model developed by Nagarajaiah and Ferrell (1999) and its effectiveness in predicting the dynamic response of elastomeric bearings is evaluated and verified using experimental data from the study by Sanchez et al (2012). The key contribution of this study is to develop a detailed analytical model that is capable of modeling the nonlinear response of elastomeric bearings under extreme loads, including the capability to more accurately capture its dependence on horizontal displacement and axial loads at displacements exceeding the stability limit. The findings of this study are in clear agreement with recently reported observations by Han et al. (2013) that the rotational spring stiffness of the analytical model is the governing factor at large displacements. A new analytical model to capture the exact nature of this nonlinearity is proposed in this study.

NONLINEAR ANALYTICAL BEARING MODEL

Figure 1 shows the nonlinear analytical model developed to model the behavior of elastomeric bearings in the two-dimensional plane. It is based on the Koh and Kelly (1986) linear model, and was first enhanced and developed into a nonlinear form by Nagarajaiah and Ferrell (1999). In this study the shear and the rotational springs of the analytical model are considered to be nonlinear elastic. The nonlinearities are deduced based on observed experimental results with particular emphasis on the ability of the analytical model to predict behavior of the bearings beyond the stability limit at large displacements and axial loads.

As shown in Figure 1, the nonlinear analytical model consists of two rigid T-shaped elements connected to each other at mid-height by a shear spring and frictionless rollers. Each of the tee section is connected to the base and top section respectively via a frictionless hinge. In summary, the nonlinear analytical model considered has two degrees of freedom (DOF), the shear displacement, s, governed by the nonlinear shear spring, K_s, and rotation, θ, governed by nonlinear rotational springs of stiffness, $K_\theta/2$. The model is subjected to axial load, P, and horizontal load, F, at the top of the bearing. The top plate is free to move in both horizontal and vertical directions but restrained from rotating. When the bearing displaces in the horizontal direction by an amount u, it is a result of a shear displacement, s, and rotation, θ, of the analytical model. The horizontal displacement, u, is given by the relation

$$u = l\sin\theta + s\cos\theta \tag{1}$$

Where, l is the combined height of rubber layers and steel shims. The nonlinear horizontal stiffness of the model, K_h, is a function of the axial load, P, and the horizontal displacement, u. In the nonlinear analytical model, both the shear stiffness, K_s, and the rotational stiffness, K_θ, vary as a function of the shear deformation, s.

Equilibrium equations

The equilibrium equations of the analytical model shown in Figure 1 are given by

Shear equilibrium

$$K_s s = F\cos\theta + P\sin\theta + \frac{K_{\theta o}\delta C_\theta \theta^2}{2} \tag{2}$$

Rotational equilibrium

$$K_\theta \theta = P(l\sin\theta + s\cos\theta) + F(l\cos\theta - s\sin\theta) \tag{3}$$

Where K_s refers to the nonlinear shear stiffness of the model, K_θ is the nonlinear rotational stiffness of the model, δ is a constant of value 1 and dimensions (1/mm) and $K_{\theta o}$ is the nonlinear rotational stiffness of the model at zero shear displacement..

In the analytical model the estimated variation of shear modulus, G, with horizontal displacement is mainly captured using the variation of the nonlinear shear stiffness, K_s, with respect to shear deformation, s.

$$K_s = K_{so}\left(1 - C_s \tanh\left(\alpha \frac{s}{l_r}\right)\right) \tag{4}$$

where K_{so} refers to the shear stiffness at zero shear strain, C_s is a dimensionless constant, and α is a dimensionless constant with a value of l_r. In order to account for correct axial-load horizontal displacement behavior the nonlinear rotational stiffness of the model, $K_{\theta,}$ is considered a function of s/l_r by Nagarajaiah and Ferrell (1999).

$$K_\theta = K_{\theta o}\left(1 - C_\theta \frac{s}{l_r}\right) \tag{5}$$

where $K_{\theta o}$ refers to the nonlinear rotational stiffness at zero shear strain and C_θ is a dimensionless constant.

The horizontal stiffness of the bearings K_h is a function of horizontal displacement, u, and axial load, P. The equilibrium paths for a given set of input parameters (C_s, C_θ, K_{so}, and $K_{\theta o}$) are solved using Runge-Kutta method to obtain values of s and θ corresponding to the applied horizontal load, F, and vertical load, P. The ability of the proposed analytical model to predict the behavior of elastomeric bearings when subjected to seismic loads is evaluated in the sections that follow.

EXPERIMENTAL RESULTS

Experiments by Sanchez et al. (2012) examined the stability limit of four different types of elastomeric bearings using the University of Buffalo NEES equipment site. Three of the types of bearings are low damping natural rubber bearings and the fourth include a lead plug. The bearings were subjected to both quasi-static and dynamic tests, the main emphasis of the experimental verifications done in this paper focus on dynamic tests. More details on the quasi-static experimental program can be found in Sanchez (2010) and Sanchez et al. (2012) while Masroor et al. (2012) provide detailed results on the dynamic stability tests. Among the bearing test results considered, six bearings belong to the same category with two subjected to quasi-static tests and the remaining four subjected to dynamic tests. The properties of the six bearings obtained from initial characterization tests are listed in Table 3. The properties listed include the effective shear modules, G_{eff}, and the effective damping ratio, β, computed from 0.1 Hz cyclic test data at 100% shear strain for two different axial loads. This data provides some insight into the dependence of the bearing behavior on axial load and also the variation in bearing properties for the six nominally identical bearings.

Quasi-static stability tests

Quasi-static stability tests were performed on the bearings using the Single Bearing Test Machine (SBTM) designed by Sanchez et al. (2012). The test setup has the ability to simultaneously apply horizontal deformations and axial loads. Two different testing methods were used to evaluate the stability of bearings. Method 1 applied a predetermined initial displacement to the bearing that remains constant while the axial load is increased monotonically from zero to a point where the horizontal force resistance of the bearing becomes zero. This approach was first proposed by Buckle et al. (2002) and Nagarajaiah and Ferrell (1999). In Method 2, a predetermined initial axial load is applied to the bearing and the horizontal displacement of the bearing is increasing monotonically from zero to a point where the horizontal force resistance of the bearing becomes zero. Only the results from Method 2 are considered here. The results obtained using Method 2 for two different bearings (labeled 15180 and 15196) are shown in Figure 2. The nonlinear nature of the force displacement curves is clearly evident from the figure and in addition it is also apparent there exists considerable variation in experimental results from two nominally identical bearings.

Dynamic Tests

The dynamic stability tests, (Sanchez et al. 2012) subjected a rigid mass supported on four bearings shown in Figure 3 to unidirectional extreme ground motions, driving the system beyond the stability limit. Though instability in bearings was earlier encountered unexpectedly by researchers (Buckle and Kelly 1986; Griffith et al. 1987), these experiments mark the first attempt undertaken to specifically gain an insight into the bearing dynamic stability under realistic loading conditions. The four bearings (with properties listed in Table 1) supported a total gravity load of 226.86 kN and were bolted to the base frame above and load cells below. The load cells were used to measure the horizontal and the vertical loads acting on each individual bearing. These four bearings used for dynamic testing were not subjected to the aforementioned quasi-static stability tests due to potential damage to the elastomer, hence the properties of the bearings from both tests vary slightly.

In the dynamic tests, the ground motions listed in Table 2 were applied at increasing intensity. The most intense ground motion proved to be the 85% MCE Erzincan record with the bearings exhibiting highly nonlinear behavior and pronounced excursions beyond their stability limits. The results from this particular test prove useful for calibration of the nonlinear analytical model of the bearing.

Analytical model of dynamic test setup

The dynamic test setup is modeled in the two-dimensional plane as a base isolated mass using 3 DOFs i.e. horizontal (u), vertical (v) and rotational (φ). A schematic of the test setup and the simplified model is shown in Figure 4(a) and (b) respectively. The equations of motion of the system are derived based on equilibrium of the system in each direction.

$$m_1\ddot{u}_1 + c_1\dot{u}_1 + k_1u_1 = -m_1(\ddot{u}_g + \ddot{u}) - m_1h(\ddot{\varphi}_g + \ddot{\varphi}) \tag{6}$$

$$m_b\ddot{u} + c_b\dot{u} + \tilde{k}_hu = -m\ddot{u}_g \tag{7}$$

$$I\ddot{\varphi} + m_1 h^2 \ddot{\varphi} + 2c_f b^2 \dot{\varphi} + 2k_f b^2 \varphi = -I\ddot{\varphi}_g - m_1 h^2 \ddot{\varphi}_g \quad (8)$$

$$m\ddot{v} + 2c_f \dot{v} + 2k_f v = -m(\ddot{v} + g) \quad (9)$$

An additional degree of freedom is introduced in the above equations corresponding to the mass m_1, this is done so as to incorporate the inertial term associated with this mass due to rotation. Hence m_b refers to mass of base frame, m_1 refers to the mass of the steel plates and concrete blocks above the frame and m refers to the total mass of the system. The equations of motion in the φ direction are formulated about the centre of gravity of the base frame, h hence refers to the distance between the centre of gravities of the base frame and mass m_1 located above it. b refers to a half width between the bearings (for the setup used by Sanchez et al. (2012) the value is 1219.2 mm). Since the total mass of the system is divided into two parts m_1 and m_b only for convenience the stiffness associated with m_1 i.e. k_1 is assigned a very high value. In the above set of equations I refers to the moment of inertia of base mat, k_f and c_f are the vertical stiffness and damping respectively of the bearings, $\ddot{u}_g$ and $\ddot{\varphi}_g$ are the acceleration input to the system measured using accelerometers placed on top of the shake table. The above systems of equations are solved using the unconditionally stable Newmark-Beta method.

The term $\tilde{k}_h$ refers to the combined horizontal stiffness of all four bearings of the system. It is a highly nonlinear term updated at each time step based on the magnitude of axial load acting on each bearing and the horizontal displacement. For calculation of the viscous damping coefficient c_b of the bearings an average damping ratio of 3.3% is used, this value is chosen based on the effective damping ratios, β_{eff}, of all the four bearings listed in Table 3. The specific focus of the study is to evaluate the ability of the nonlinear analytical model proposed above to model the observed experimental dynamic behavior. Since high nonlinear bearing behavior is anticipated, including considerable loss of stiffness beyond the stability limit, a corrective pseudo-force methodology developed by Nagarajaiah et al. (1991) is employed in the solution algorithm. The nonlinear forces corresponding to the bearings are represented separately as pseudoforces and at each time step an iterative corrective pseudoforces methodology is employed until equilibrium is achieved and tolerance criteria are met.

Figure 5 shows a plan view of the test setup with identification label for each bearing. The input excitation is applied in the east-west direction. An insight into the horizontal force-displacement, $F - u$, behavior of the bearings is not possible without resolving the coupled horizontal-vertical behavior of the bearings. Since the focus of this paper is only to gain an insight into the horizontal behavior, the vertical dynamics are accounted for by using experimentally recorded values of vertical load at each of the bearings. The coupled horizontal-vertical behavior of the bearings needs to be addressed, and is the subject of further research. In this study, the nonlinear horizontal stiffness of each bearing is calculated at every time step based on the experimental value of vertical load, P, recorded at that instant and the horizontal displacement, u, calculated from the solution algorithm. Hence, when equations (6-9) are solved, at each time step the vertical reaction at each bearing is updated based on experimentally recorded values. The total horizontal force imparted by the four bearings is labeled f_b, the contributions from bearings on the left side of the test setup (#1 and #3) are labeled $f_{b,l}$ and on the right side of the test setup (#2 and #4) are labeled $f_{b,r}$.

INPUT PARAMETERS

The shear stiffness of the bearings at zero shear strain, K_{so}, is obtained directly from experimental results by differentiating the horizontal force, F, with respect to horizontal displacement, u, as shown below. In order to obtain accurate values of K_{so} the horizontal force – displacement, $F - u$, curve obtained using Method 2 for an axial load, P, of zero kN is chosen.

$$K_{so} = K_{h[exp]}(0, u) = \left.\frac{dF}{du}\right|_{P=0} \tag{10}$$

The experimental response of all four bearings of the test setup when subjected to 20% MCE Erzincan ground motion is shown in Figure 6. The difference in the stiffness of all four bearings is evident from this figure. The value of K_{so} for all the four bearings is estimated based on the horizontal force – displacement, F – u, curve for low values of u. From Table 3, the mechanical properties of the four bearings used in the dynamic vary slightly, with, additional variation in stiffness due to the uneven distribution of axial loads on the four bearings.

In an earlier study by Nagarajaiah and Ferrell (1999), the variation of shear modulus, G, was taken into account using the dimensionless constant C_s = 0.325. It is possible to estimate the value of C_s with greater accuracy due to the detailed experimental results available. The stiffness of the bearing can be determined by differentiating F (from Method 2 data for a constant value of P) with respect to u. At very small values of u, the rotation of the analytical model is negligible. The main factor that governs the behavior of K_h is shear stiffness K_s, which in turn is dependent on the value of C_s. Figure 7 shows the accuracy of C_s in estimating the normalized stiffness curves compared to experimental values evaluated using horizontal force – displacement, F – u, curves obtained from quasi-static test Method 2 for P = 0 kN. From Table 3 it can be seen that the value of G_{eff} of bearing 15180 is high compared to all the other bearings (15196 and bearings #1 – 4) hence the value of C_s = 0.2821 (determined from bearing 15196, Figure 7) is used for the analytical model.

All the other input parameters of the nonlinear analytical model are calculated according to the following relations (Buckle and Kelly 1986; Koh and Kelly 1986; Nagarajaiah and Ferrell 1999). The effective flexural rigidity is calculated based on the approximation

$$(EI)_{eff} = E_r I \frac{l}{l_r} \tag{11}$$

Where, E_r is estimated as

$$E_r = E_o(1 + (2/3)S^2) \tag{12}$$

The elastic modulus of rubber, $E_o = 4G_o$, I is the moment of inertia of the bearing about the axis of bending, and S is the shape factor defined as

$$S = \frac{(D_o - D_i)}{4 \times t_r} \tag{13}$$

In the equation above, D_o and D_i are the outer diameter of the bearing and the diameter of the mandrel hole and t_r is the thickness of each rubber layer of the bearing.

$K_{\theta o}$ is estimated as follows

$$K_{\theta o} = \frac{\pi^2 (EI)_{eff}}{l} = \frac{\pi^2 E_r I}{l_r} \tag{14}$$

The dimensionless constant, C_θ, is estimated based on the physically motivated formula dependent on the rubber layer thickness of the bearings (Nagarajaiah and Ferrell 1999).

$$C_\theta = \alpha C'_\theta = l_r \left(\frac{t_u}{D_o} - \frac{t_r}{D_o} \right)$$

(15)

where, t_u refers to rubber layer of unit thickness, l_r is the total thickness of the rubber and α is a dimensionless constant with a value of l_r.

Adequacy of the Nagarajaiah and Ferrell (1999) model for dynamic loads

The emphasis of an earlier study (Nagarajaiah and Ferrell 1999) was to develop an analytical model that is able to capture the post-critical behavior of elastomeric bearings observed experimentally. In light of the experimental results provided by Sanchez et al.(Sanchez et al. 2012), the ability of the Nagarajaiah and Ferrell (1999) model to predict the response of the bearings is evaluated. Figure 8 shows the simulated response of the bearings for 85% MCE Erzincan ground motion. It is evident that the analytical model is not predicting the stability limit and stiffness degradation beyond this point accurately. The stiffness of the bearings beyond the stability limit is greater than that predicted by the analytical model indicating that the bearings have additional reserve capacity to recover from instability. Nagarajaiah and Ferrell (1999) model was based on quasi-static tests of bearings carried out under controlled loading conditions, the results of the experiments presented here were carried out under dynamic conditions where the bearings are free to move without being influenced by any predetermined loading condition.

Proposed analytical model

At large values of u, the governing factor for K_h is the variation of K_θ, this observation is in agreement with recent findings by Han et al. (2013). The current formulation where K_θ is defined as a linear function of s/l_r is clearly not sufficient. Thus, the formulation is modified by incorporating higher order terms of s/l_r and redefining K_θ as follows

$$K_\theta = K_{\theta o}\left(1 - C_\theta\left(\frac{s}{l_r}\right) - C_{\theta 1}\left(\frac{s}{l_r}\right)^2 - C_{\theta 2}\left(\frac{s}{l_r}\right)^3\right) \tag{16}$$

where $C_{\theta 1}$ and $C_{\theta 2}$ are dimensionless parameters. These parameters are estimated based on the response of the bearings to 85% MCE Erzincan ground motion. A three dimensional plot of stiffness of the bearings as a function of axial load, P, and horizontal displacement of the bearing, u, is shown in Figure 9.

Since all the four bearings differ in their properties, the input parameters corresponding to each of the bearing models are also varied accordingly. The input parameters of the new model proposed in this study are estimated based on the response of the bearings to Erzincan ground motion. The accuracy of the model is then verified using ground motion not considered for estimation of input parameters; namely Kobe and Newhall ground motion. For initial estimates of K_{so}, data from 20% MCE Erzincan ground motion is used with the analytical model proposed by Nagarajaiah and Ferrell(1999). For estimating the dimensionless parameters $C_{\theta 1}$ and $C_{\theta 2}$, 85% MCE Erzincan ground motion is considered along with the new analytical model proposed in this study. As described and demonstrated earlier in Figure 8, the stiffness of the bearings beyond the stability limit predicted by Nagarajaiah and Ferrell (1999) model degrades too rapidly. A more gradual descent in stiffness is desired in order to better capture the response of the bearings both at and beyond the stability limit. The input parameters for all four bearings estimated based on Erzincan ground motion are listed in Table 4. In Figure 10 a comparison is made between the K_θ obtained from Nagarajaiah and Ferrell (1999) model and the new analytical model proposed above for a constant value of axial load, P, acting on the bearing.

Figure 11 shows the force – displacement, $F – u$, response of the bearings subjected to 20% MCE level of the Erzincan ground motion and Figure 12 shows the time history response of the forces experienced by the bearings and also the base displacement response predicted by the analytical model. Clearly the initial stiffness of the bearings is estimated well. Figure 13 and Figure 14 show the response of the bearings to 85% MCE level of ground motion. Simulation results are able to clearly capture the nonlinear reduction in stiffness associated with each bearing at and beyond the stability limits. In Figure 13, the drop in stiffness at the instant of instability is captured well; however, the loop width of the simulated response differs from that of experimental response indicating greater energy dissipation in the experiment.

During dynamic testing, Masroor et al. (2012) observed gradual and minimal change in the properties of the bearings as ground motion intensities are increased. The largest change was recorded occurred after the 85% MCE Erzincan input motion, indicating approximately 10% drop in shear modulus and 13% increase in damping ratio of the bearings. These changes occurred because of damage to the bearings after reaching large strains beyond the instability limit in first cycle of the Erzincan ground motion. In this study those changes have not been deliberately incorporated, hence the stiffness of bearings differ slightly from observed experimental results (#1 and #4 bearings in Figure 13). This is the reason for the discrepancy in shear response prediction of bearings #1 and #4 observed from the time histories presented in Figure 14. In spite of these discrepancies, the base displacement is captured well using the new analytical model shown in Figure 14, especially the peak values. Under service conditions, bearing properties vary with time with some of these changes difficult to monitor. It is hence important to evaluate if the analytical model developed in this study is capable of predicting the response despite these small changes in their properties. The ability of the analytical model in capturing the response of the bearings to varying intensity levels of Erzincan ground motion is shown in Figure 15. For brevity, only two bearings (#1 and #2) are presented, since the other bearings experienced similar displacements and axial load variations as the bearings on the same side along the testing direction. The accuracy of the analytical model is demonstrated for various MCE levels of Erzincan ground motion.

VERIFICATION OF MODEL FOR OTHER GROUND MOTIONS

For verification purposes experimental results for Kobe and Northridge, Newhall ground motions are used. The results of the analytical model are presented next.

Kobe ground motion

Simulated response of the bearings for Kobe ground motion of intensity 20%, 40%, 67% and 100% MCE level are shown in Figure 16 for bearings #1 and #2. It can be seen that the stiffness of the bearings has been well estimated at all intensities of ground motion. The peak values of shear forces in all four bearings and the peak base displacements are also captured well as shown as the intensity of the ground motion increases from 20% to 100% MCE level. The closeness of the fit between predicted and experimentally observed response is demonstrated.

Newhall ground motion

Simulated response of bearings for Newhall ground motion for 20%, 40% and 100% MCE levels are shown in Figure 17 (for bearings #1 and #2). The analytical model predicts the response well at all ground intensities. The reduction in stiffness observed in the bearings for 100% MCE level of Newhall ground motion is more pronounced when compared to its response for 100% Kobe ground motion and the analytical model is able to capture it well.

For comparison purposes, the response of the bearings for 100% MCE level Kobe and Newhall ground motions are simulated using the Nagarajaiah and Ferrell (1999) model and presented for bearings #1 and

#2 in Figure 18. It is evident that the earlier model proposed by Nagarajaiah and Ferrell (1999) is unable to model the response accurately once the bearing reaches the stability limits. In Figure 19 the quasi-static stability curves are plotted along with the dynamic response of the bearings to 85% MCE Erzincan ground motions. Force – displacement, $F - u$, curves obtained from bearing 15196 using quasi-static test Method 2 for axial loads 44.48 and 88.96 kN are presented in Figure 19 and compared to the dynamic response of bearing (bearing #1 for 85% MCE Erzincan) with axial load variation that lies within this range. It is clear from the plot that the available quasi-static test data only provide information up to the stability limit.

DISCUSSION AND CONCLUSION

From the experimental results presented, it is clear that the stiffness degradation of the elastomeric bearings beyond the stability limit is not predicted accurately by earlier models (Nagarajaiah and Ferrell 1999). The analytical model proposed in this study clearly captures the observed behavior of the bearings at lower intensities with very high accuracy. At higher intensities (85% MCE Erzincan) where the behavior of the bearing becomes highly nonlinear in nature, despite the difference in properties of the four bearings the analytical model predicts with reasonable accuracy the critical load and captures the response for the entire extent of loss of stability of the bearings. The unique experimental results available combined with the current analytical model provide a detailed insight into the nonlinear behavior of the bearings. When the response of the bearings to the most intense ground motions is considered, it becomes apparent that the bearings exhibit significant capacity to sustain loads far beyond the static stability limit. Another important conclusion from this study is that in order to accurately capture the behavior of the bearings beyond the stability limit, analytical model parameters derived from quasi-static tests are insufficient. The dimensionless parameters $C_{\theta 1}$ and $C_{\theta 2}$ are crucial for predicting the response of the bearings observed beyond the stability limit and their values cannot be determined based on quasi-static tests alone. Though extensive experimental findings are presented in this and earlier studies by co-authors of this study, results from bearings of different geometry need to be evaluated using the current model before any general conclusions regarding the input parameters can be reached. In summary, the analytical model presented in this study gives valuable insight into the nonlinear behavior of bearings and represents the first attempt to model the nonlinear dynamic response for the entire displacement range including the region beyond the stability limit.

ACKNOWLEDGEMENTS

Authors VVSM and SN gratefully acknowledge funding support provided by grant NSF-CMMI--NEESR-0830391 for this project. AM and GM were supported by NSF-NEESR-CMMI-1113275.

REFERENCES

Bažant, Z. P. (2003). Shear Buckling of Sandwich, Fiber Composite and Lattice Columns, Bearings, and Helical Springs: Paradox Resolved. *Journal of Applied Mechanics , 70* (1), 75-83.

Bažant, Z. P., & Cedolin, L. (1991). *Stability of Structures.* New York: Oxford University Press.

Buckle, I., & Kelly, J. M. (1986). Properties of slender elastomeric isolation bearings during shake table studies of a large-scale model bridge deck. *Joint Sealing and bearing systems for concrete structures* , 247-269.

Buckle, I., Nagarajaiah, S., & Ferrell, K. (2002). Stability of Elastomeric Isolation Bearings: Experimental Study. *J. Struct. Engrg. , 128* (1), 3-11.

Cardone, D., & Perrone, G. (2012). Critical load of slender elastomeric seismic isolators: An experimental perspective. *Engineering Structures* , 198-204.

Derham, C. J., & Thomas, A. G. (1981). In *Control of seismic response of piping system and other structures.* (pp. 21-36).

Gent, A. N. (1964). Elastic stability of rubber compression springs. *J. Mech. Engrg. Sci. , 6* (4), 318-326.

Griffith, M. C., Kelly, J. M., & Aiken, I. D. (1987). *A displacement control and uplift restraint device for base isolated devices.* UCB/EERC-87/3, University of California, Berkeley, Berkeley, CA.

Han, X., Kelleher, C. A., Warn, G. P., & Wagener, T. (2013). Identification of the controlling mechanism for predicting critical loads in elastomeric bearings. *J. Struct. Engrg.* , DOI: 10.1061/(ASCE)ST.1943-541X.0000811.

Haringx, J. A. (1948). On highly compressible helical springs and rubber rods and their application for vibration-free mountings. I. *Phillips Res. Rep. , 3*, 401-449.

Haringx, J. A. (1949). On highly compressible helical springs and rubber rods and their application for vibration-free mountings. II. *Phillips Res. Rep., , 4*, 49-80.

Haringx, J. A. (1949). On highly compressible helical springs and rubber rods and their application for vibration-free mountings. III. *Phillips Res. Rep. , 4*, 206-220.

Iizuka, M. (2000). A macroscopic model for predicting large-deformation behaviors of laminated rubber bearings. *Engineering Structures* , 323-334.

Kikuchi, M., Nakamura, T., & Aiken, I. D. (2010). Three-dimensional analysis for square seismic isolation bearings under large shear deformations and high axial loads. *Earthquake Engng Struct. Dyn. , 39*, 1513-1531.

Koh, C. G., & Kelly, J. M. (1988). A simple mechanical model for elastomeric bearings used in base isolation. *International Journal of Mechanical Sciences , 30* (12), 933-943.

Koh, C. G., & Kelly, J. M. (1986). *Effects of axial load on elastomeric bearings.* University of California, Berkeley. Berkeley, CA: Earthquake Engineering Research Center.

Koh, C. G., & Kelly, J. M. (1989). Viscoelastic Stability Model for Elastomeric Isolation Bearings. *J. Struct. Engrg. , 115* (2), 285-302.

Masroor, A., Sanchez, J., Mosqueda, G., & Ryan, K. L. (2012). Dynamic Stability of Elastomeric Bearings at Large Displacement. *Proceedings of 15th World Conference on Earthquake Engineering.* Lisbon, Portugal.

Nagarajaiah, S., & Ferrell, K. (1999). Stability of Elastomeric Seismic Isolation Bearings. *J. Struct. Engrg. , 125* (9), 946-954.

Nagarajaiah, S., Reinhorn, A. M., & Constantinou, M. C. (1991). Nonlinear dynamic analysis of 3-d-base-isolated structures. *J. Struct. Engrg. , 117* (7), 2035-2054.

Sanchez, J. (2010). *Stability of elastomeric bearings for seismic applications.* MS Thesis, Department of Civil, Structural and Environmental Engineering, State University of New York, Buffalo.

Sanchez, J., Masroor, A., Mosqueda, G., & Ryan, K. L. (2012). Static and Dynamic Stability of Elastomeric Bearings for Seismic Protection of Structures. *J. Struct. Engrg.* , DOI: 10.1061/(ASCE)ST.1943-541X.0000660.

Warn, G. P., & Weisman, J. (2011). Parametric finite element investigation of the critical load capacity of elastomeric strip bearings. *Engineering Structures , 33* (12), 3509-3515.

Weisman, J., & Warn, G. P. (2012). Stability of Elastomeric and Lead-Rubber Seismic Isolation Bearings. *J. Struct. Engrg. , 138* (2), 215-223.

Table 1: Properties of the bearings tested by Sanchez et al. (2012)

Schematic of the bearing	Properties of the bearing

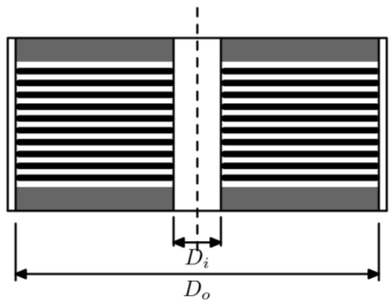

Shape Factor, S	10.64
Height (mm)	163.07
Outside diameter, D_o (mm)	165.1
Inside diameter, D_i (mm)	29.97
Thickness of rubber, t_r (mm)	3.175
Number of rubber layers, n_r	25
Area, $A_b = \pi/4(D_o^2 - D_i^2)$ (mm^2)	20702.9
G_{eff} at 25% (MPa)	0.60
G_{eff} at 100% (MPa)	0.46

Table 2: List of selected ground motions used for dynamic testing by Sanchez et al. (2012)

Ground Motion Record	Station	Magnitude (M_w)	Scaled PGA (g)	MCE scale factor	Test intensities (% MCE)	Used in this study for
1992 Erzincan – Erzincan Station	ERZ-NS	6.69	0.87	1.76	20, 40, 67, 85	Calibration
1995 Kobe – Takatori	TAK090	6.90	0.55	0.89	20, 40, 67, 100	Verification
1994 Northridge – Newhall Fire station	NWH360	6.69	0.86	1.46	20, 40, 100	Verification

Table 3: Effective shear modulus, G_{eff}, and damping ratio, β_{eff}, at 100% shear strain for bearing used in experimental study.

		G_{eff} (MPa)		β_{eff} (%)	
Axial Load (kips)		10	14	10	14
Test Type	Bearing ID				
Quasi Static	15196	0.531	0.476	3.2	3.8
Quasi Static	15180	0.579	0.524	2.8	3.1
Dynamic	#1 – NW	0.524	0.386	3.2	3.4
Dynamic	#2 – NE	0.545	0.414	3.1	3.3
Dynamic	#3 – SW	0.524	0.407	3.2	3.4
Dynamic	#4 – SE	0.531	0.407	3.1	3.2

Table 4: Parameters for the four bearings in the dynamic tests for the new analytical model

	$C_{\theta 1}$	$C_{\theta 2}$	K_{so} (kN/mm)
Original values	-0.0977	0.0136	
Bearing	Multiplication factors		
1	1.00	1.00	0.1869
2	1.12	1.33	0.1682
3	1.28	1.22	0.1159
4	0.88	1.11	0.2468

figure 1

Click here to download Figure: figure 1.pdf

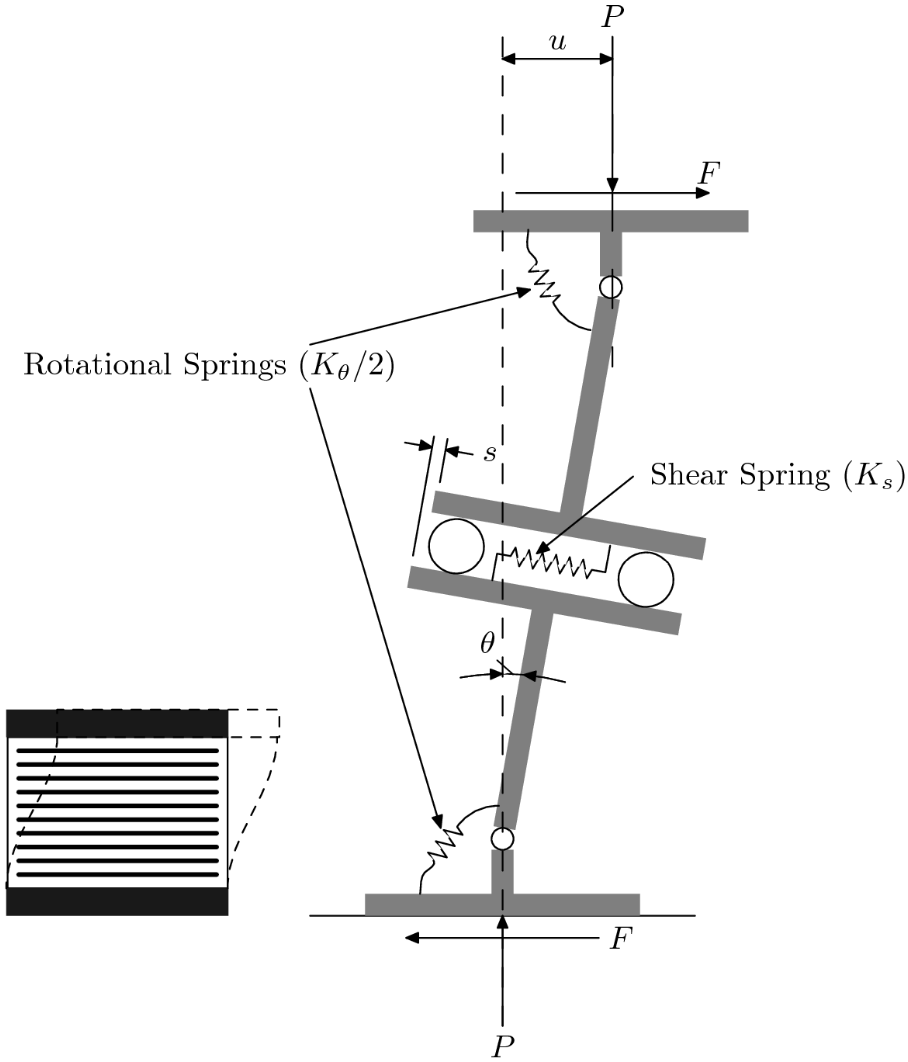

(a) Elastomeric bearing (b) Analytical model (not to scale)

Figure
Click here to download Figure: figure 2.pdf

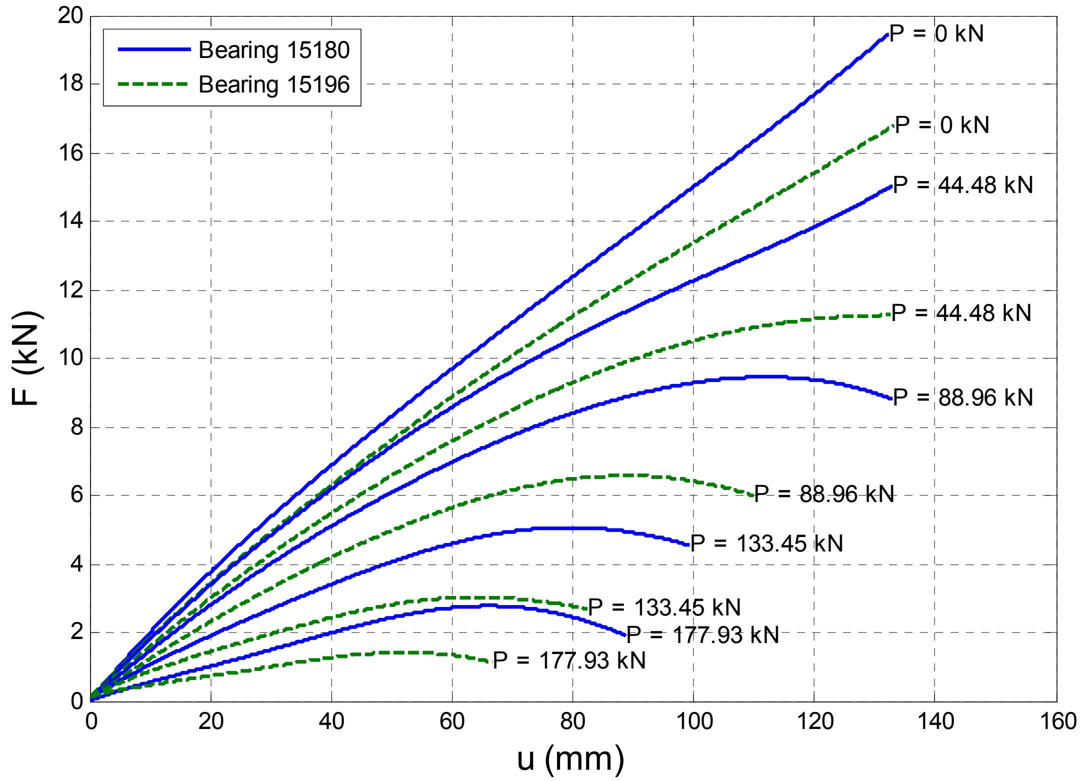

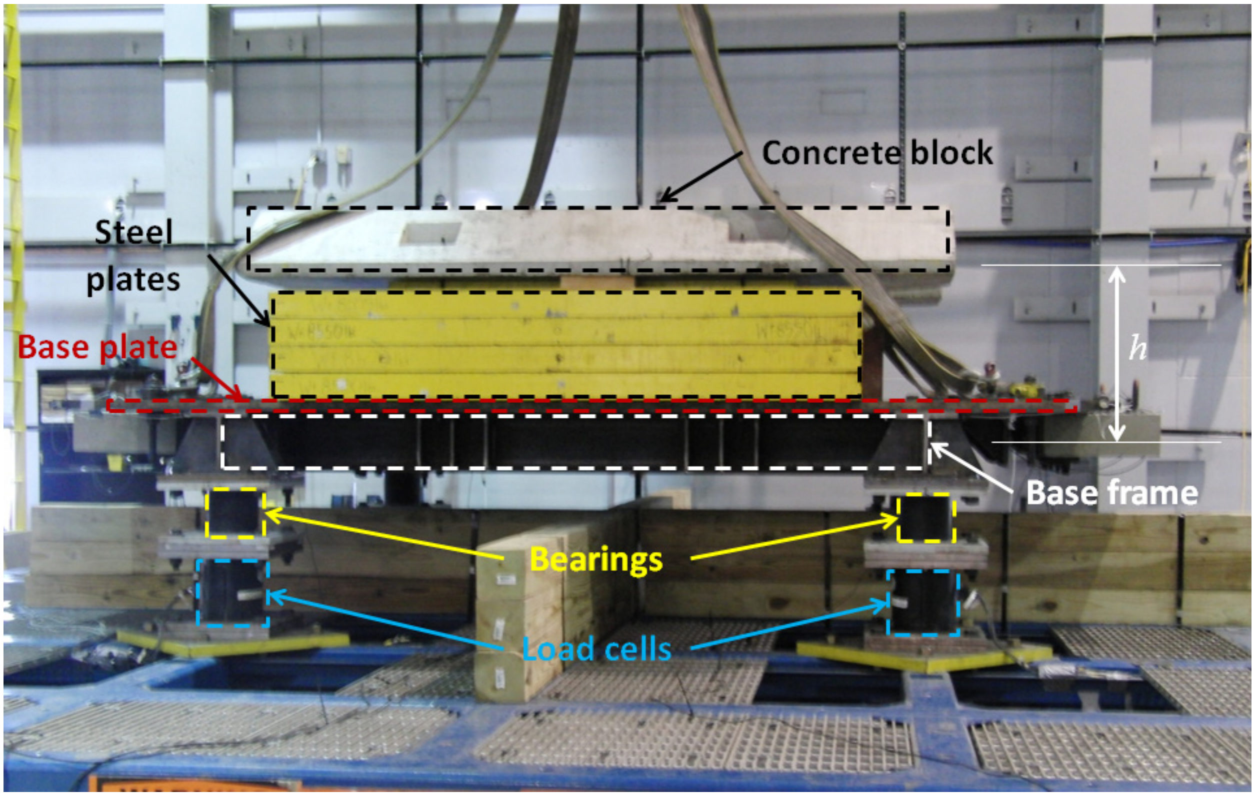
Concrete block
Steel plates
Base plate
h
Base frame
Bearings
Load cells

Figure
Click here to download Figure: figure 4.pdf

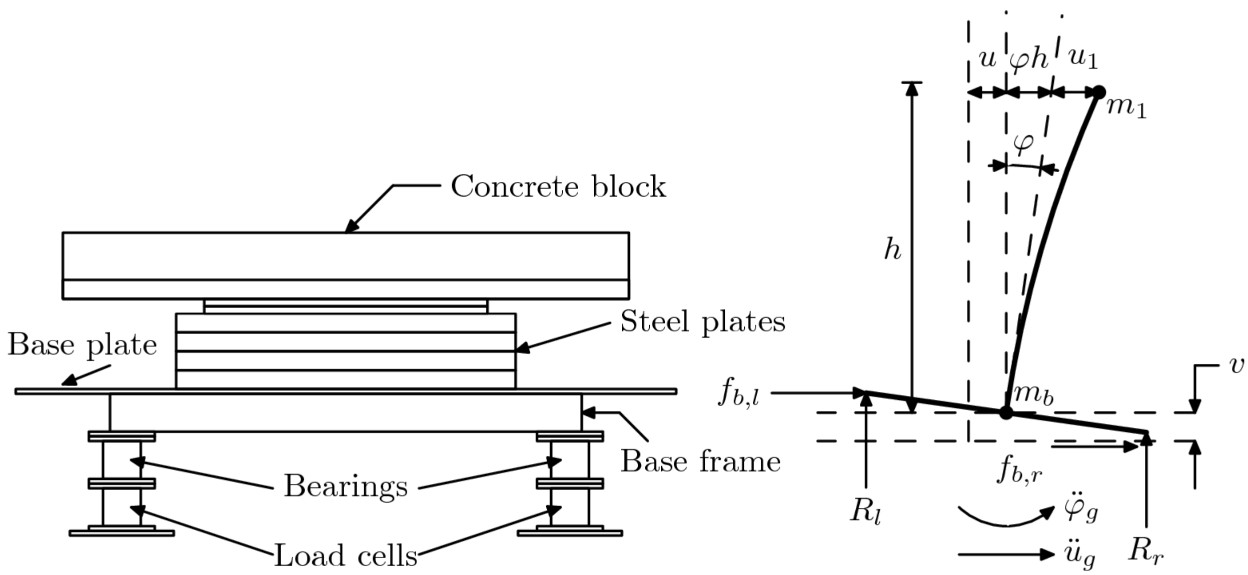

(a) Test setup (b) Deformed model(not to scale)

Figure
Click here to download Figure: figure 5.pdf

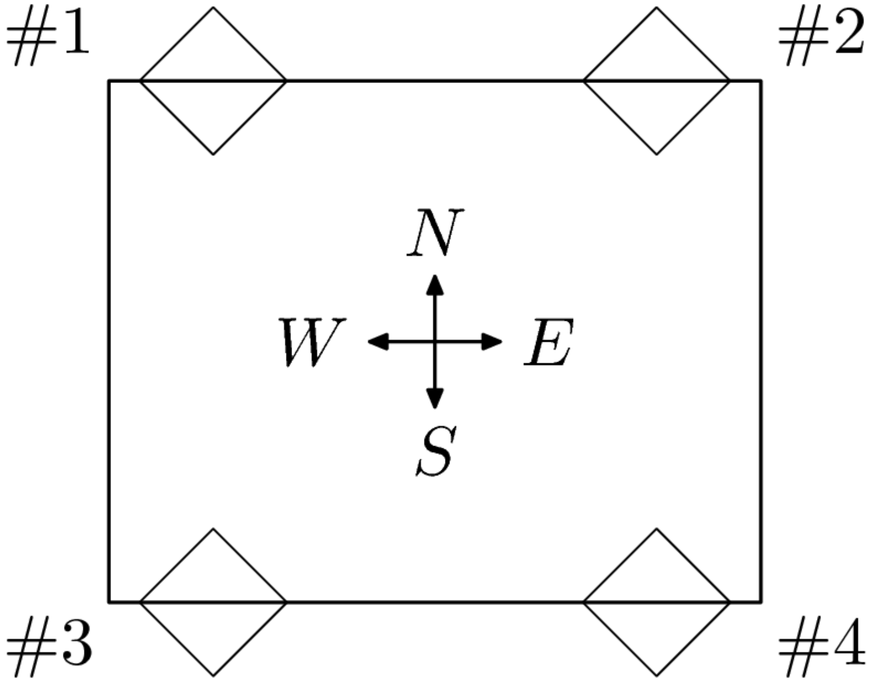

Figure
Click here to download Figure: figure 6.pdf

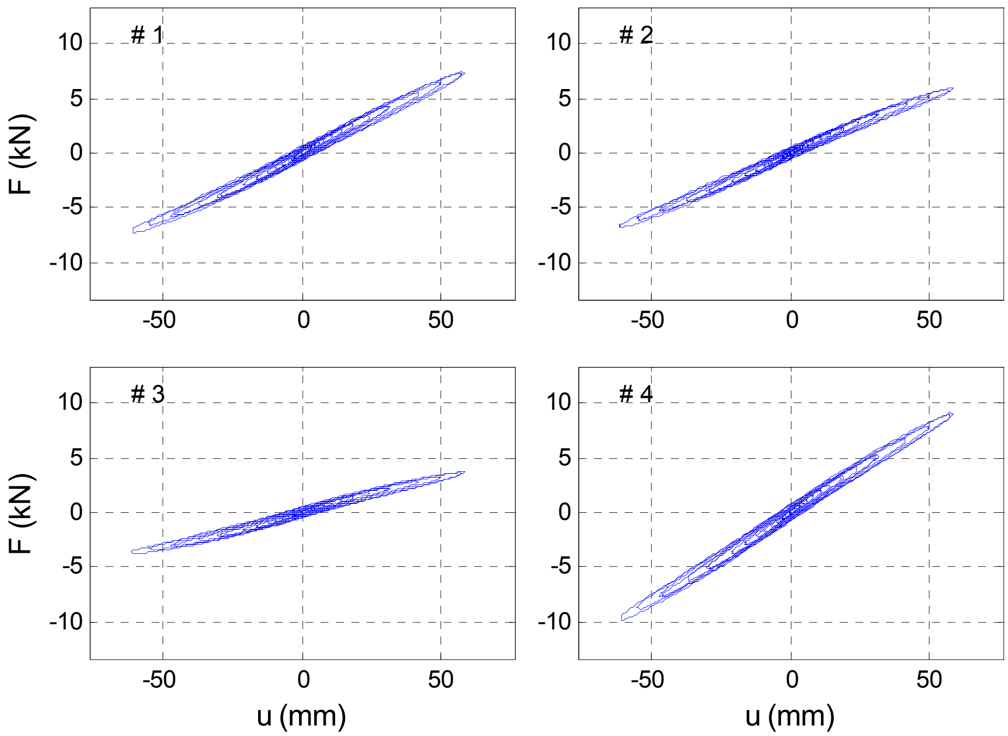

Figure

Click here to download Figure: figure 7.pdf

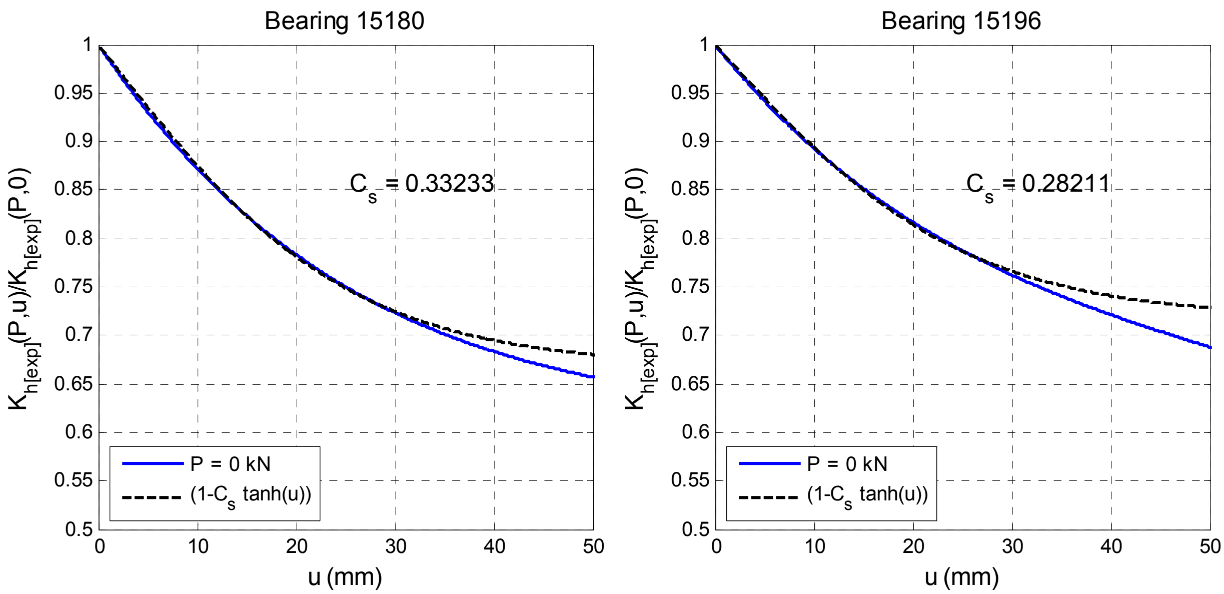

Figure
Click here to download Figure: figure 8.pdf

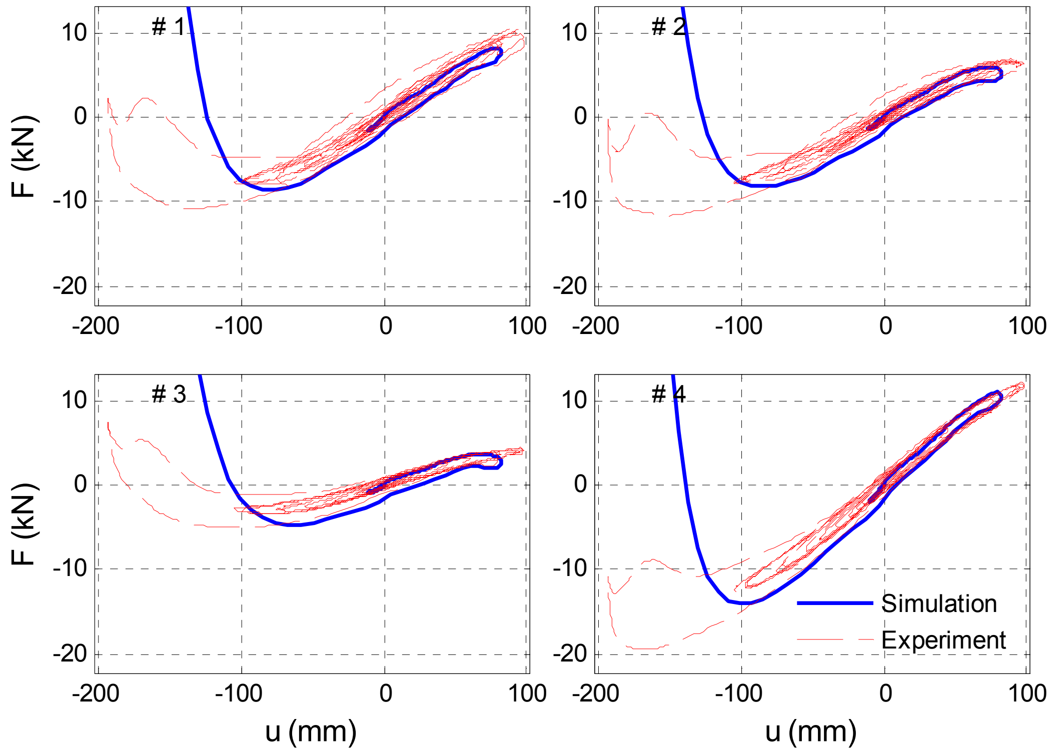

Figure

Click here to download Figure: figure 9.pdf

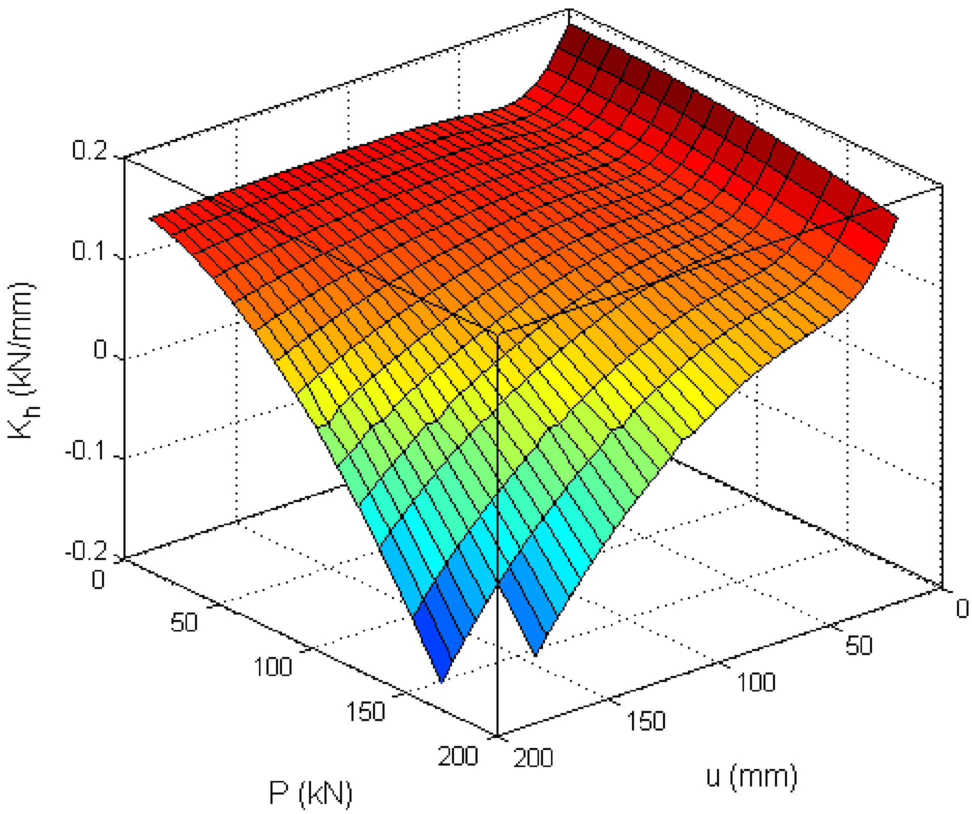

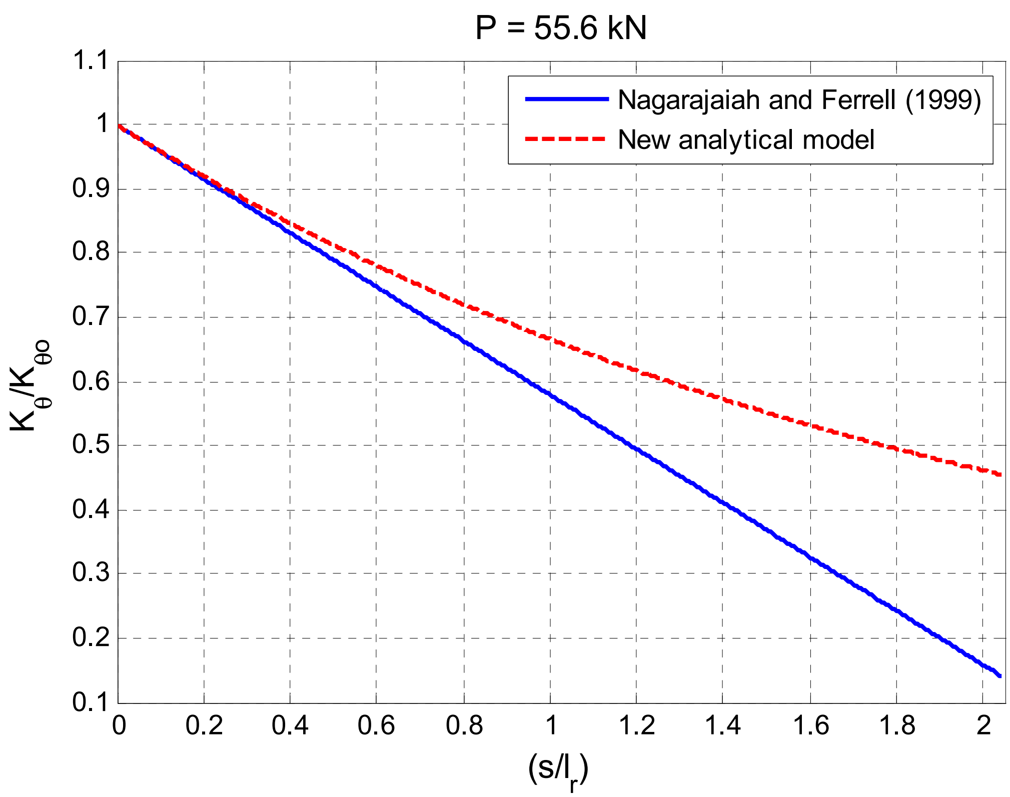
P = 55.6 kN
Nagarajaiah and Ferrell (1999)
New analytical model
$K_\theta/K_{\theta o}$
(s/l_r)
1.1
1
0.9
0.8
0.7
0.6
0.5
0.4
0.3
0.2
0.1
0
0.2
0.4
0.6
0.8
1
1.2
1.4
1.6
1.8
2

Figure

Click here to download Figure: figure 11.pdf

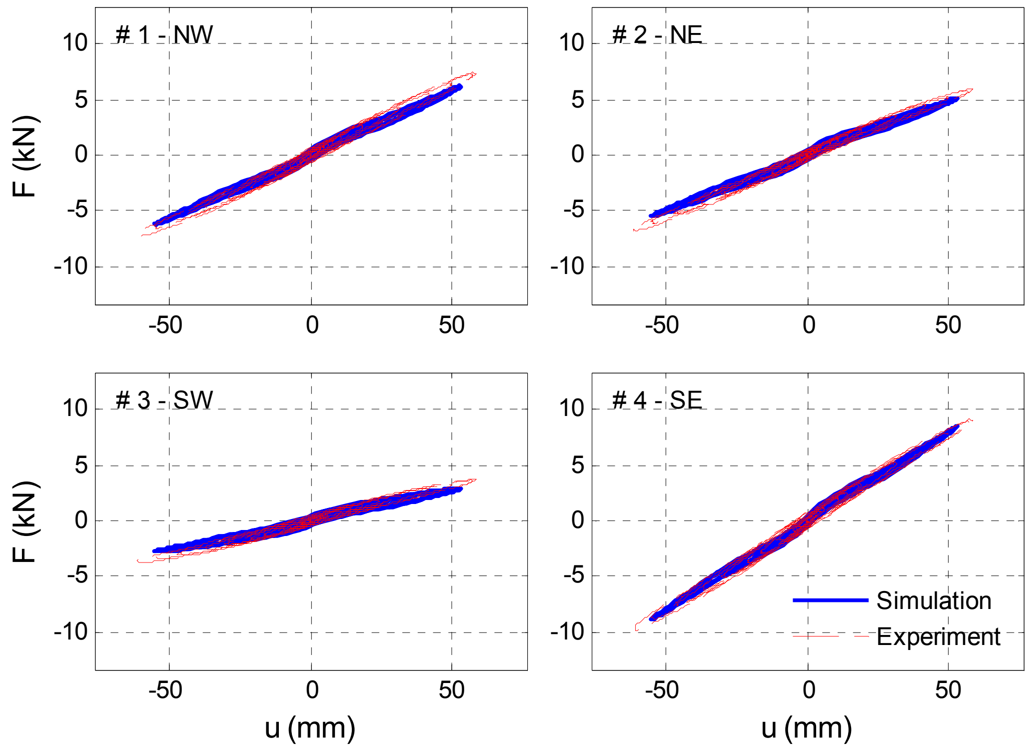

Figure

Click here to download Figure: figure 12.pdf

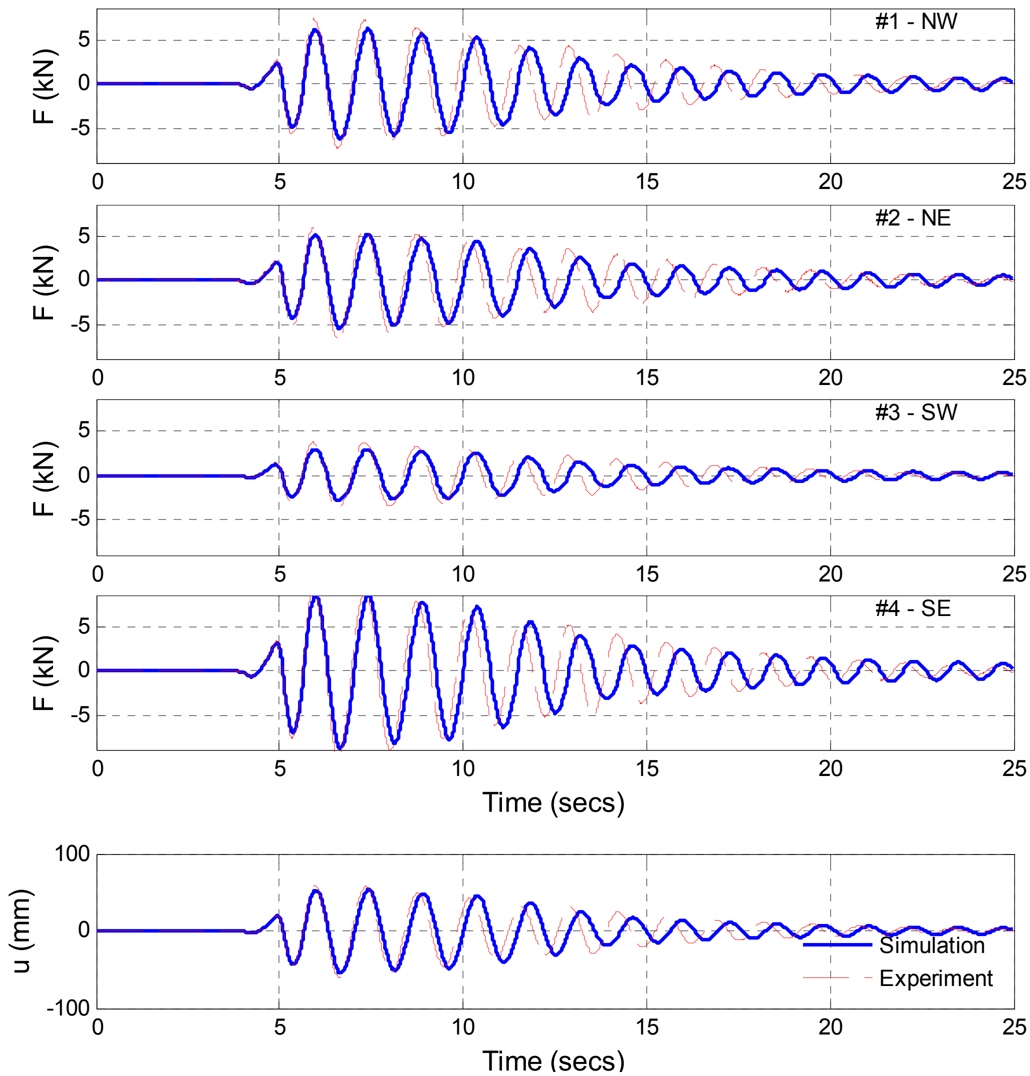

Figure
Click here to download Figure: figure 13.pdf

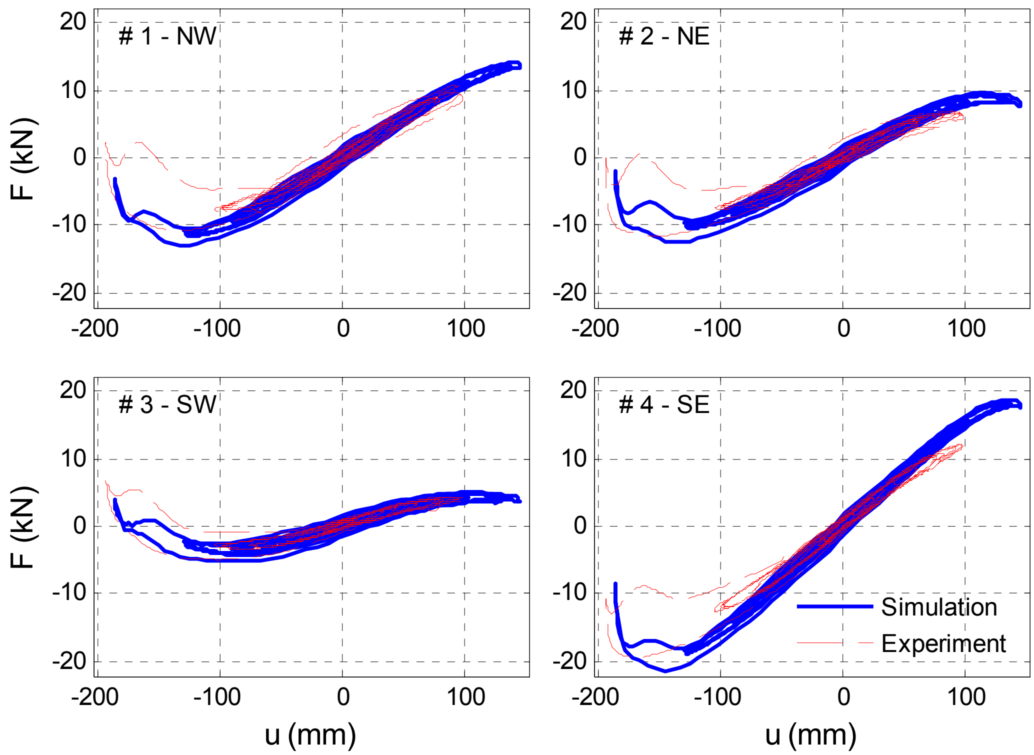

Figure

Click here to download Figure: figure 14.pdf

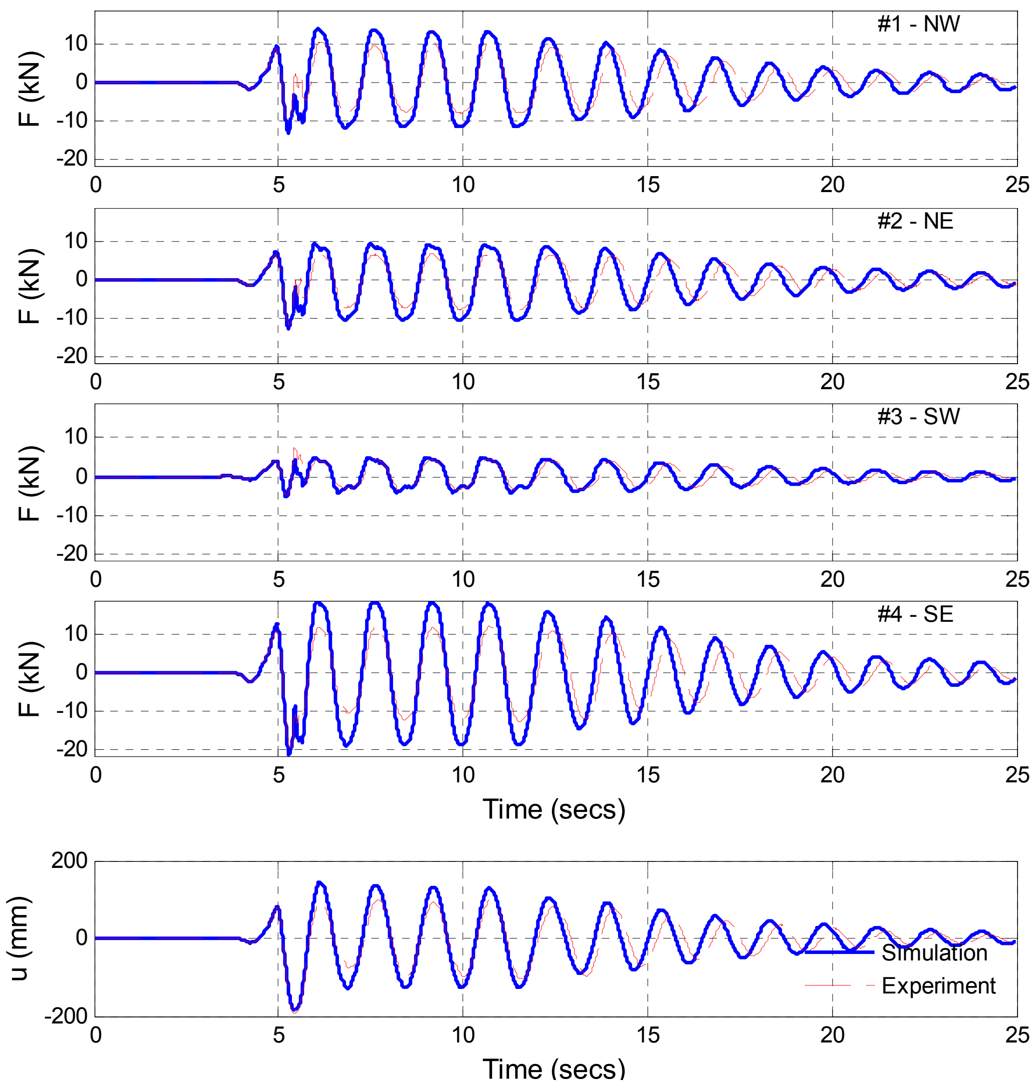

Figure
Click here to download Figure: figure 15.pdf

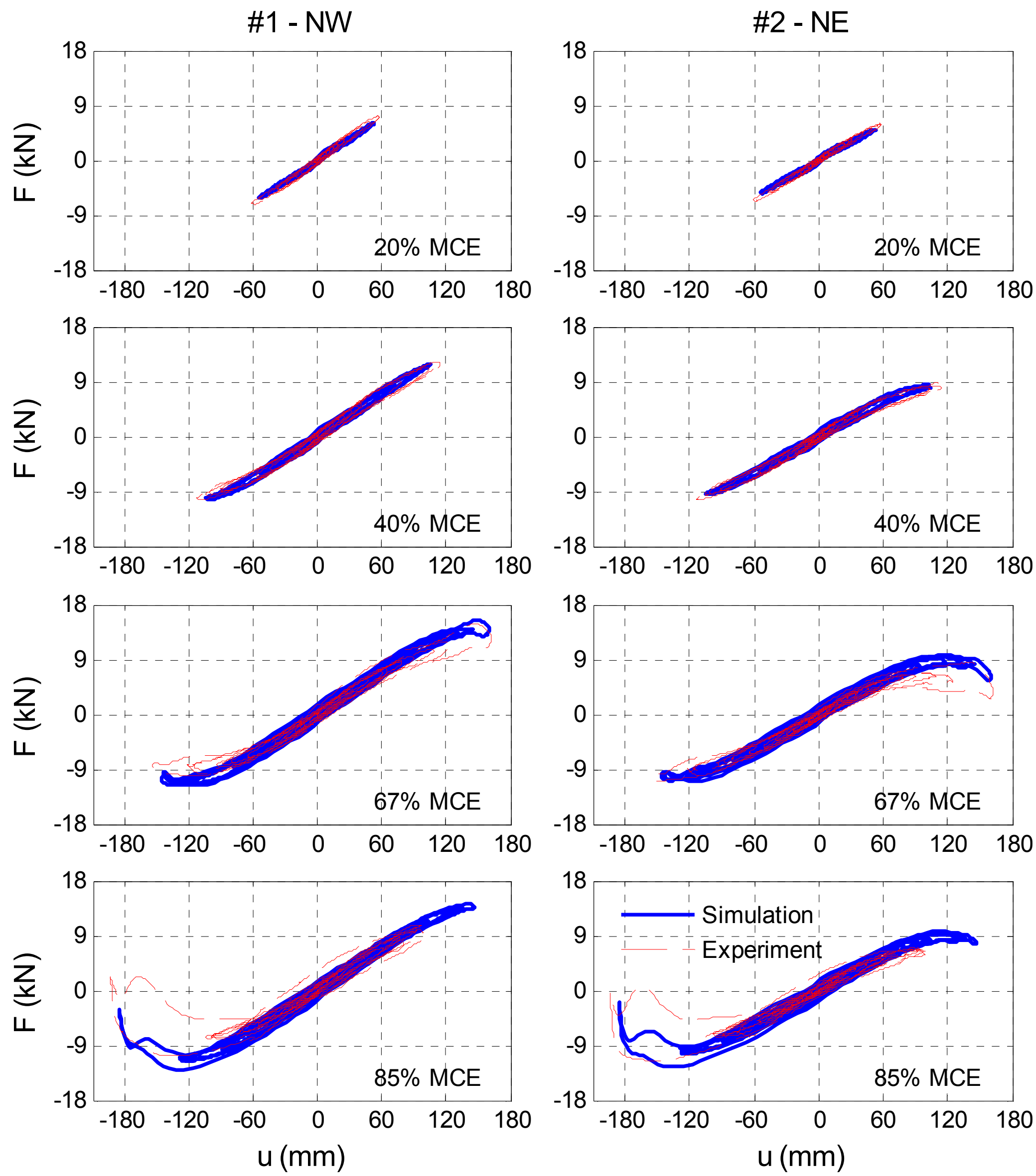

Figure
Click here to download Figure: figure 16.pdf

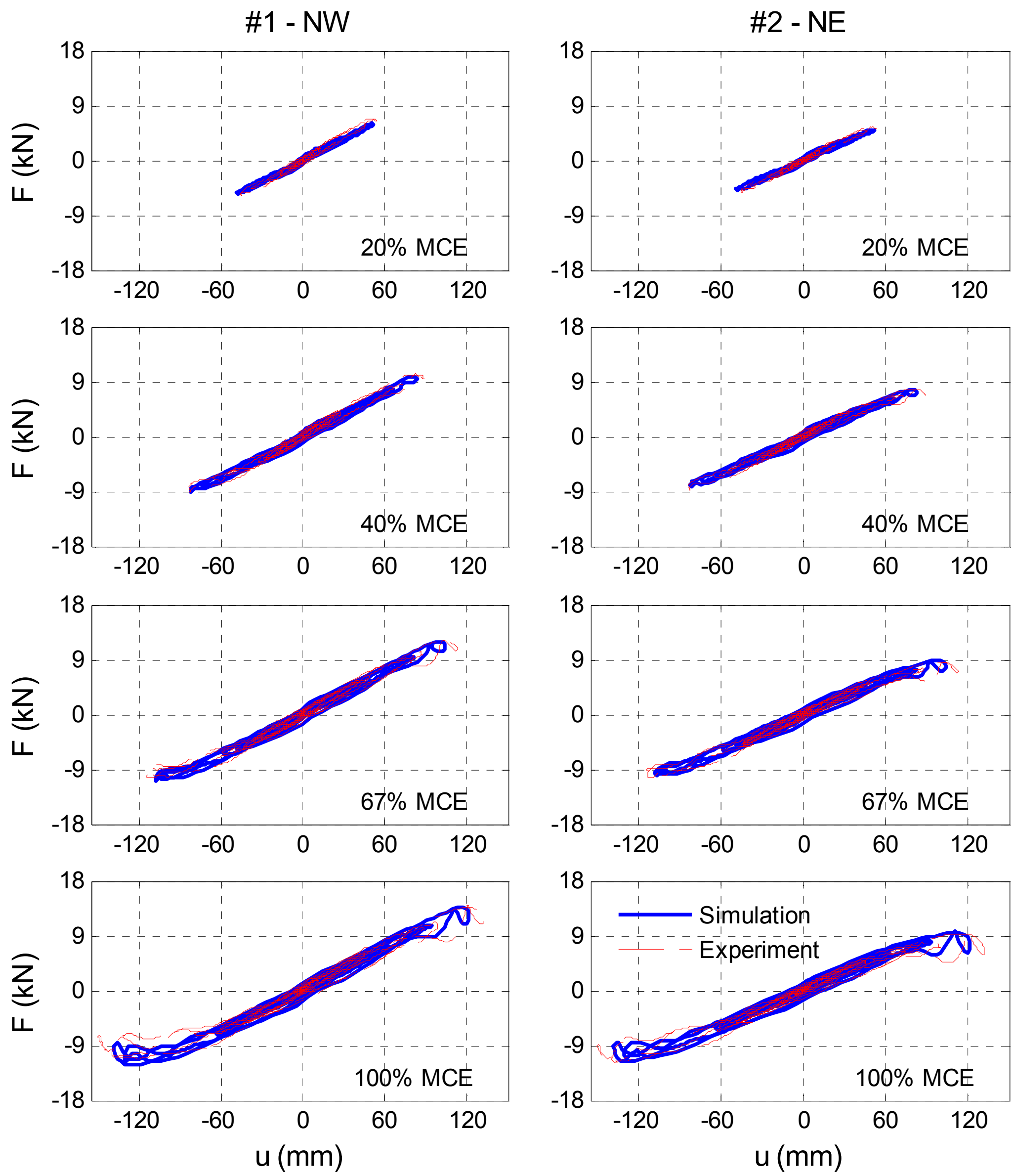

Figure
Click here to download Figure: figure 17.pdf

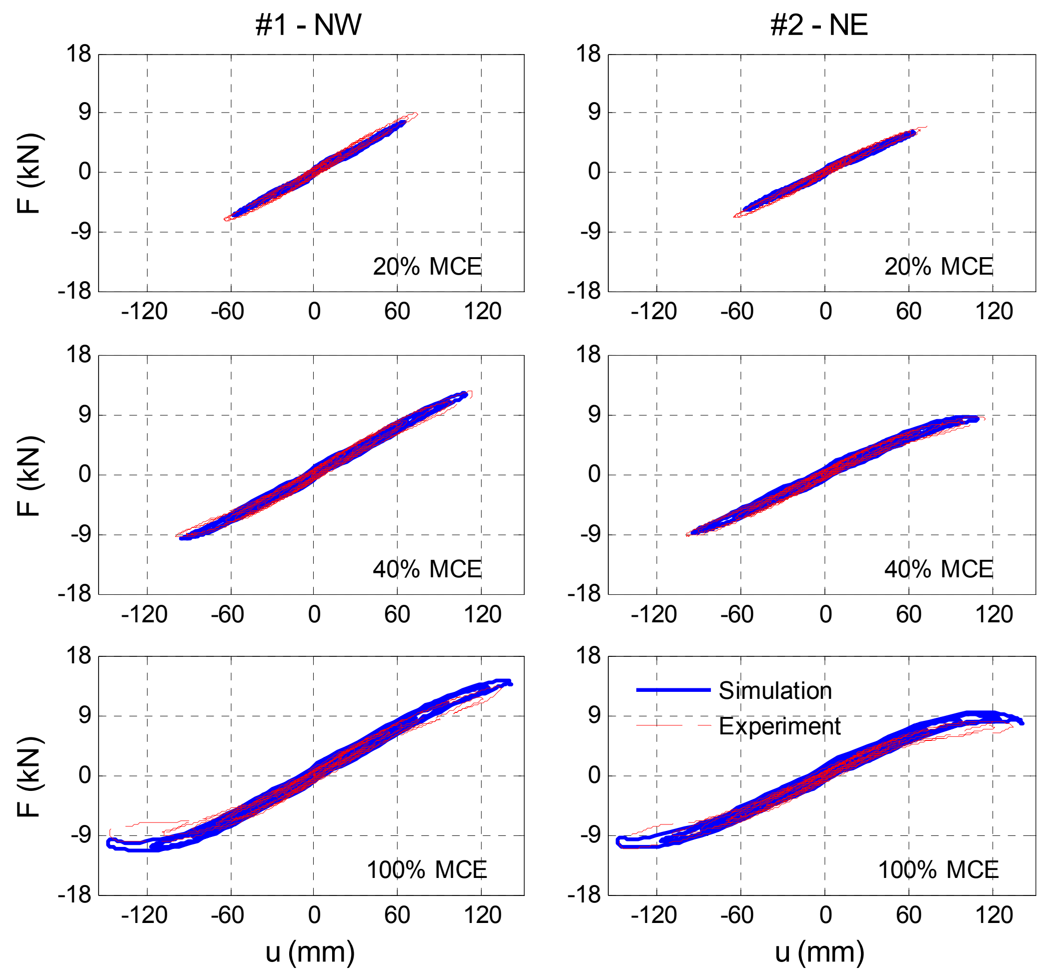

Figure
Click here to download Figure: figure 18.pdf

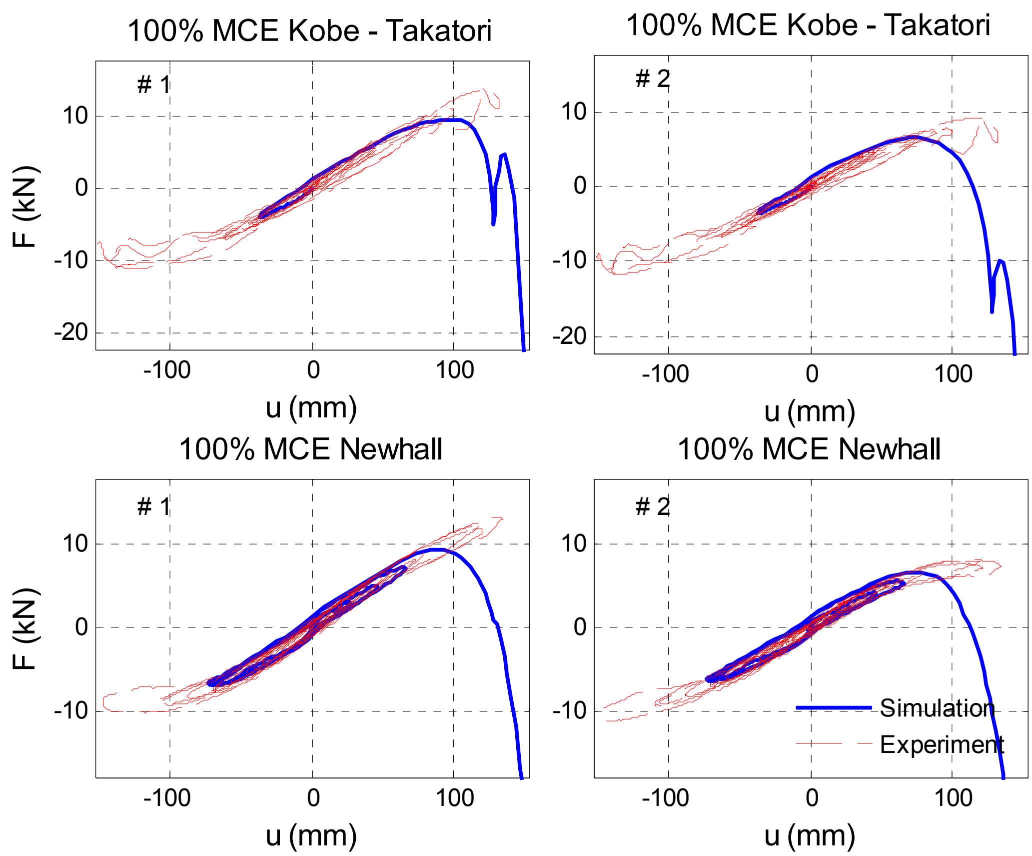

Figure
Click here to download Figure: figure 19.pdf

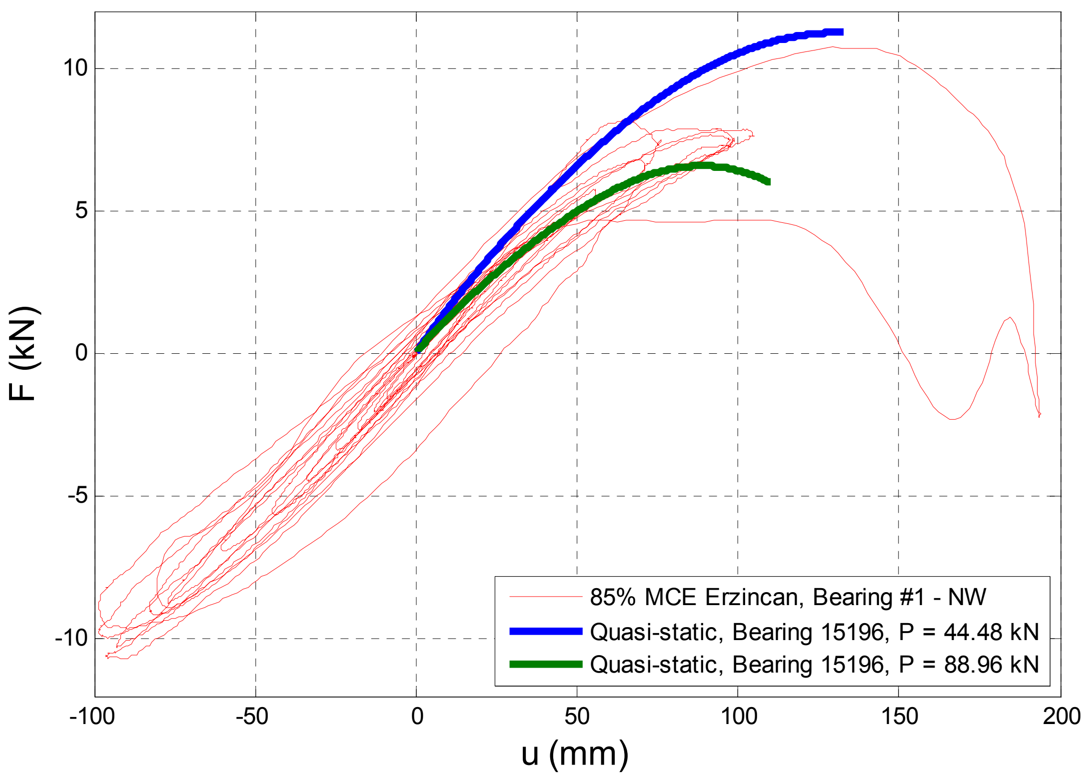

Figure 1: Nonlinear analytical model used in this study

Figure 2: Force - displacement behavior of two different bearings (15180 and 15196) obtained by quasi-static stability test Method 2.

Figure 3: Test setup used for dynamic loading of bearings

Figure 4: Schematic of the experimental setup and analytical model used to simulate its response

Figure 5: Top view of the test setup

Figure 6: Experimental force – displacement, $F – u$, response of the four bearings subjected to 20% MCE Erzincan ground motion

Figure 7: Normalized horizontal stiffness as a function of horizontal displacement obtained experimentally from horizontal force – displacement, $F – u$, curves for P = 0 kN and analytically based on estimated value of C_s for bearings 15180 and 15196.

Figure 8: Simulated horizontal force – displacement, $F – u$, response of the bearings using model by Nagarajaiah and Ferrell (1999) when subjected to 85% MCE Erzincan ground motion

Figure 9: Three dimensional plot of stiffness of the bearing, K_h, as a function of axial load, P, and horizontal displacement, u, generated using the new analytical model.

Figure 10: Normalized plot of rotational stiffness, K_θ, as a function of shear displacement, s, obtained from the model by Nagarajaiah and Ferrell (1999) and the new analytical model

Figure 11: Simulated horizontal force – displacement, $F – u$, response of the bearings using new analytical nonlinear model when subjected to 20% MCE Erzincan ground motion

Figure 12: Simulated time histories of horizontal force, F, in all the four bearings and base displacement, u, using new analytical nonlinear model when subjected to 20% MCE Erzincan ground motion

Figure 13: Simulated horizontal force – displacement, $F – u$, response of the bearings using new analytical nonlinear model when subjected to 85% MCE Erzincan ground motion

Figure 14: Simulated time histories of horizontal force, *F*, in all the four bearings and base displacement, *u*, using new analytical nonlinear model when subjected to 85% MCE Erzincan ground motion

Figure 15: Simulated and experimental horizontal force – displacement, *F* – *u*, loops of bearings #1 and #2 when subjected to 20%, 40%, 67% and 85% MCE level Erzincan ground motion.

Figure 16: Simulated and experimental horizontal force – displacement, *F* – *u*, loops of bearings #1 and #2 when subjected to 20%, 40%, 67% and 100% MCE level Kobe - Takatori ground motion.

Figure 17: Simulated and experimental horizontal force – displacement, *F* – *u*, loops of bearings #1 and #2 when subjected to 20%, 40% and 100% MCE level Newhall ground motion.

Figure 18: Simulated and experimental horizontal force – displacement, F – u, loops of bearings #1 and #2 when subjected to 100% MCE level Kobe and Newhall ground motions using the Nagarajaiah and Ferrell (1999) model.

Figure 19: Response of Bearing #1 to 87% Erzincan ground motion and quasi-static force – displacement, *F* - *u*, curves from bearing 15196 for axial loads of 44.48 and 88.96 kN.